Outdoor field performances of Insect-based visual motion sensors

Fabien Expert, Stéphane Viollet, Franck Ruffier

Outdoor field performances of insect-based visual motion sensors

Fabien Expert, Stéphane Viollet and Franck Ruffier

Biorobotics Department - Institute of Movement Science

CNRS / Aix-Marseille University

CP938 - 163 av Luminy F-13288 Marseille, France

{fabien.expert, stephane.viollet, franck.ruffier}@univmed.fr

Abstract

Considerable attention has been paid during the last decade to navigation systems based on the use of visual optic flow cues. Optic flow-based visuo-motor control systems have been implemented on an increasingly large number of sighted autonomous robots designed to travel under specific lighting conditions. Many algorithms based on conventional cameras or custom-made sensors are being used nowadays to process visual motion. In this paper, we focus on the reliability of our optical sensors which can be used to measure the local 1-D angular speed of robots flying outdoors over a visual scene in terms of their accuracy, range, refresh rate and sensitivity to illuminance variations. We have designed, constructed and characterized two miniature custom-made visual motion sensors: (i) the APIS-based local motion sensor involving the use of a custom-made VLSI array (APIS stands for "Adaptive Pixels for Insect-based Sensors"), which is equipped with Delbrück-type auto-adaptive pixels, and (ii) the LSC-based (LSC is a component purchased from iC-Haus) local motion sensor involving the use of off-the-shelf linearly amplified photosensors, which is equipped with an on-chip pre-amplification circuit. By combining these photodetectors with a low-cost optical assembly and a bio-inspired visual processing algorithm, highly effective miniature sensors were obtained for measuring the visual angular speed in field experiments. The present study focused on the static characteristics and the dynamic responses of these local motion sensors over a wide range of illuminance values, ranging from 50lux to 10000lux both indoors and outdoors. Although outdoors experiments are of great interest to equip Micro-Air Vehicles with visual motion sensors, we also performed indoors experiments as a comparison. The LSC-based visual motion sensor was found to be more accurate in a narrow 1.5-decade illuminance range, while the APIS-based visual motion

sensor is more robust to illuminance changes in a larger 3-decade range. The method presented in this study provides a new benchmark test for thoroughly characterizing visual motion and optic flow sensors designed to operate outdoors under various lighting conditions, in unknown environments where future Micro-Aerial Vehicles will be able to navigate safely.

1 Introduction

Several optic flow-based navigation systems have been developed during the last decade for use onboard terrestrial and aerial robots.

Some terrestrial robots are now being equipped with similar means of detecting and processing the optic flow to those providing insects such as flies and bees with the vital cues they need to control their own trajectories (Franceschini, Pichon & Blanes, 1992; Harrison & Koch, 1999; Humbert & Hyslop, 2010; Zwaan & Santos-Victor, 1999). Systems of this kind have even been recently used to make flying robots able to avoid obstacles (Beyeler, Zufferey & Floreano, 2009; Green, Oh & Barrows, 2004; Iida, 2001; Ruffier & Franceschini, 2008; Zufferey & Floreano, 2006), hover (Herisse, Russotto, Hamel & Mahony, 2008; Kendoul, Nonami, Fantoni & Lozano, 2009), track a moving target (Kendoul et al., 2009; Kerhuel, Viollet & Franceschini, 2010; Viollet & Franceschini, 1999) and take off, follow a terrain and land (Franceschini, Ruffier & Serres, 2007; Ruffier & Franceschini, 2005).

We have subdivided these visual motion sensors sensitive to optic flow cues into two categories, as follows:

- 1-D local motion sensors, which are based on a one dimensional (1-D) retina and compute a 1-D angular speed,
- 2-D photosensor arrays, which resolve the optic flow vector by measuring its 2 orthogonal components, the so-called 2-D optic flow sensors.

Many methods of measuring the visual angular speed have been used for robotic purposes, such as those involving the local 1-D Hassenstein and Reichardt correlator (Hassenstein & Reichardt, 1956), which was mounted on terrestrial robots (Harrison & Koch, 1999; Liu & Usseglio-Viretta, 2001), the Interpolation Image Algorithm (I2A) (Srinivasan, 1994) combined with a 1-D camera array, which was used onboard an indoor microflyer (Zufferey & Floreano, 2006), and the "time of travel" scheme (Blanes, 1986) combined with off-the-shelf photodiodes, which was implemented on both a terrestrial robot (Franceschini et al., 1992) and several tethered flying robots (Netter & Franceschini, 2002; Ruffier & Franceschini, 2005; Ruffier, Viollet, Amic & Franceschini, 2003; Viollet & Franceschini, 2001).

In addition, some indoor terrestrial robots (Etienne-Cummings, 1999; Santos-Victor, Sandini, Curotto & Garibaldi, 1995) have been equipped with standard cameras combined with navigation systems based on optic flow principles (see (Barron, Fleet & Beauchemin, 1994) for a review of the main optic flow techniques). Off-the-shelf computer mouse sensors measuring local 2-D optic flow were recently characterized (Chan, Mulla & Stol, 2010) and mounted onboard terrestrial (Dahmen, Millers & Mallot, 2009; Jackson, Callahan & Marstrander, 2007) and aerial robotic platforms (Beyeler et al., 2009; Griffiths, Saunders, Curtis, Barber, McLain & Beard, 2006) navigating under constant lighting conditions.

Other visual motion sensors have been developed using analog and digital Very-Large-Scale Integration (VLSI) technology (see (Barrows & Neely, 2000; Brinkworth, Shoemaker & O'Caroll, 2009; Orchard, Bartolozzi & Indiveri, 2009; Sarpeshkar, Bair & Koch, 1993; Xu, Humbert & Abshire, 2011) in the case of 1-D motion sensors, (Higgins & Shams, 2002; Sarpeshkar, Kramer, Indiveri & Koch, 1996) in the case of 2-D optic flow sensors, and see also (Mead, 1989; Moini, 1999) for a general review). Some other VLSI sensors based on the use of optic flow cues have been developed for collision detection purposes, such as that (Laviana, Carranza, Vargas, Linan & Roca, 2005) inspired by the locust.

However, to our knowledge, very few robotic studies have been published so far in which visual motion sensors have been implemented and tested outdoors, where the illuminance cannot be easily controlled (see (Barrows & Neely, 2000) for linear 1-D motion sensors and see (Beyeler et al., 2009; Garratt & Chahl, 2008; Griffiths et al., 2006; Kendoul, Yu & Nonami, 2010) for 2-D optic flow sensors).

Although visual motion sensors are of great interest for robotic applications, very few attempts have been made so far to characterize systems of this kind. Some authors have tested their visual motion sensors with virtual objects presented on a video screen (using a 1-D local motion sensor (Moeckel & Liu, 2007) or 2-D optic flow sensors (Díaz, Ros, Agis & Bernier, 2008; Okuno & Yagi, 2009)) and the performances of some VLSI motion sensors have been described in detail (see (Brinkworth et al., 2009; Harrison & Koch, 1999) for a 1-D motion sensor characterized indoors and in front of photographs of natural scenes, respectively, and see (Stocker, 2006) for a 2-D optic flow sensor characterized indoors).

It therefore seemed to be worth developing means of testing the reliability of the visual motion systems developed at our laboratory in terms of their resolution, accuracy, sensitivity and invariance to contrast in real environments under a large range of illuminance values. In this study, it was proposed to determine and compare the output signals of two custom-made bio-inspired 1-D local motion sensors (Viollet, Ruffier, Ray, Menouni, Aubépart, Kerhuel & Franceschini, 2010) based on a 2-pixel system with different front-ends, namely:

1. The APIS-based local motion sensor involving the use of a custom-made VLSI array (APIS stands for

"Adaptive Pixels for Insect-based Sensors") equipped with Delbrück-type auto-adaptive pixels (Delbrück & Mead, 1994), and

2. The LSC-based local motion sensor involving the use of off-the-shelf linearly amplified photosensors (the LSC component was purchased from iC-Haus) equipped with an on-chip pre-amplification stage.

Our visual motion scheme processes the time elapsing between the detection of any contrasting feature by two adjacent photoreceptors (Blanes, 1986, 1991; Franceschini et al., 1992; Franceschini, Ruffier, Serres & Viollet, 2009; Ruffier et al., 2003): this scheme was originally inspired by the fly's Elementary Motion Detector neurons (EMDs), since studies in which individual optical micro-stimulations were applied successively to two adjacent fly photoreceptors showed that "the first contrast change is able to facilitate the response to the second contrast change" (Franceschini, Riehle & Nestour, 1989): these responses were recorded electro-physiologically in the fly's large tangential H1 neuron. This local motion processing system belongs to the token-matching category of schemes (Ullman, 1981) and was later called the "time of travel" scheme (Benson & Delbrück, 1992; Moeckel & Liu, 2007). In the mid-1990's, a similar principle was used again to design a smart VLSI circuit called the "facilitate and sample" sensor (Kramer, Sarpeshkar & Koch, 1995).

The characteristics of the two local motion sensors in question were determined here by recording their responses to a purely rotational optic flow generated by rotating the sensors mechanically indoors and outdoors. In the case of a stationary environment, the rotational optic flow ω, which is by definition independent of the distance from the sensors to the surrounding objects (Koenderink & van Doorn, 1987), can be directly compared to the rate gyro output signal denoted Ω_{gyro}.

In this study, we also analysed the refresh rate of our local motion sensors, as this is a key parameter in optic flow-based robotic applications. The average refresh rate $\overline{f_{refresh}}$, was defined here as the number of new visual motion measurements obtained per second: a new measurement occurred whenever a contrast was detected by the first pixel and then by the second pixel with a time lag corresponding to our measurement range. The refresh rate was computed and analysed under various illuminance conditions, both indoors and outdoors.

A description of the two local motion sensors tested here is given in section II. Section III gives an account of the performances of these visual motion sensors, which were tested both indoors and outdoors in a large range of illuminance levels. For the sake of clarity, constant thresholds and settings were applied throughout this study: the performances of both visual motion sensors were found to be remarkably satisfactory in terms of their accuracy, refresh rate and robustness to changes in the visual environment and the illuminance.

The LSC-based visual motion sensor proved to work more efficiently in terms of the refresh rate and the accuracy in a narrow dynamic range of 1.5 decades, whereas the APIS-based visual motion sensor measured the angular speed accurately in a much wider 3-decade range of illuminance values.

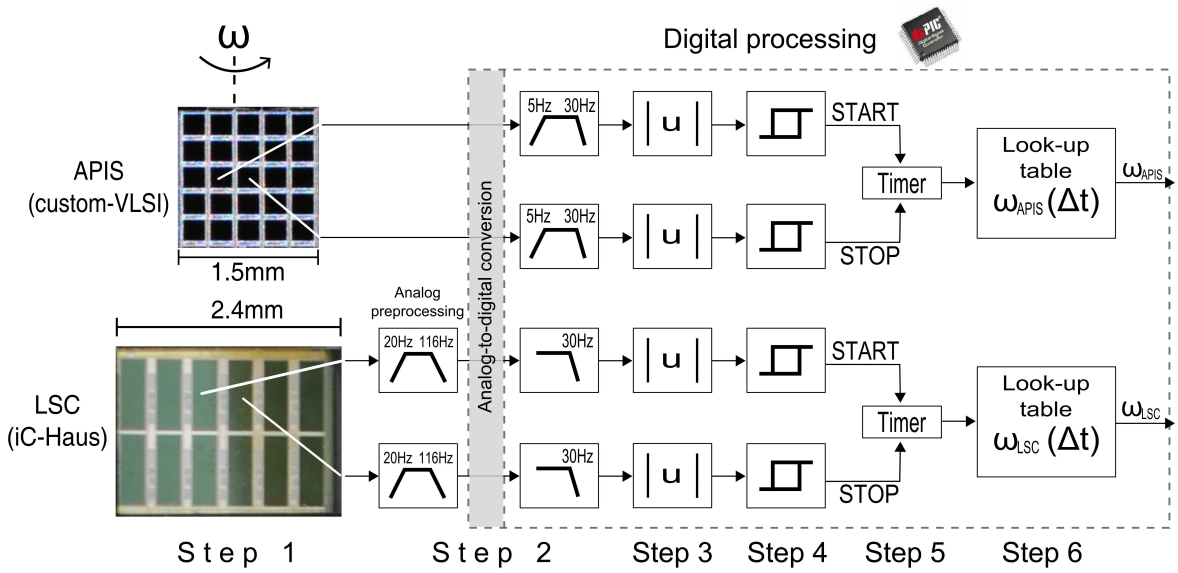

Figure 1: General processing architecture of the APIS-based and LSC-based local motion sensors. In each sensor, the output signals emitted by two adjacent pixels were spatially and temporally filtered and thresholded to determine the angular speed ω. The "time of travel" scheme previously developed at Franceschini's Laboratory (Blanes, 1986, 1991; Franceschini et al., 2009) was used to measure the local visual motion. The angular speed measured by each sensor ω_{meas} is the ratio between the constant inter-receptor angle $\Delta\varphi$ and the time Δt elapsing between the first and second thresholded signals. The overall processing of the two local motion sensors was carried out in parallel on the same microcontroller (dsPIC 33FJ128GP804) at a sampling frequency of 2kHz.
In the case of the LSC-based motion sensor, the two photodiode outputs were first filtered by an analog band-pass filter with cut-off frequencies [20Hz, 116Hz] before being filtered by a digital second order low-pass filter with a cut-off frequency of 30Hz.
In the case of the APIS-based motion sensor, the two photodiode outputs were filtered by a digital band-pass filter with cut-off frequencies [5Hz, 30Hz].

2 Description of the local visual motion sensors

Basically, each of the APIS-based and LSC-based visual motion sensors consists of a lens placed in front of a photosensor array: each visual motion sensor processes the output signals generated by 2 photodiodes. Each photodiode's output signal is transmitted to a processing unit, where a digital version of the visual motion algorithm assesses the relative angular speed ω of any contrasting features encountered in the environment (i.e., a 1-D component of the optic flow). In this study, two 2-pixel motion sensors based on the same "time of travel" principle but equipped with two different front-ends were compared (see figure 2).

The front-end of the APIS-based local motion sensor was based on adaptive pixels, originally suggested by (Delbrück & Mead, 1994). The whole APIS (Adaptive Pixels for Insect-based Sensors) retina, a custom-made VLSI retina comprising 25 pixels (figure 2d), was developed in collaboration with the Center for Particle Physics (CPPM) in Marseilles (Aubépart, Ménouni, Loubignac, Dinkelspieler & Franceschini, 2007; Viollet et al., 2010). Each pixel

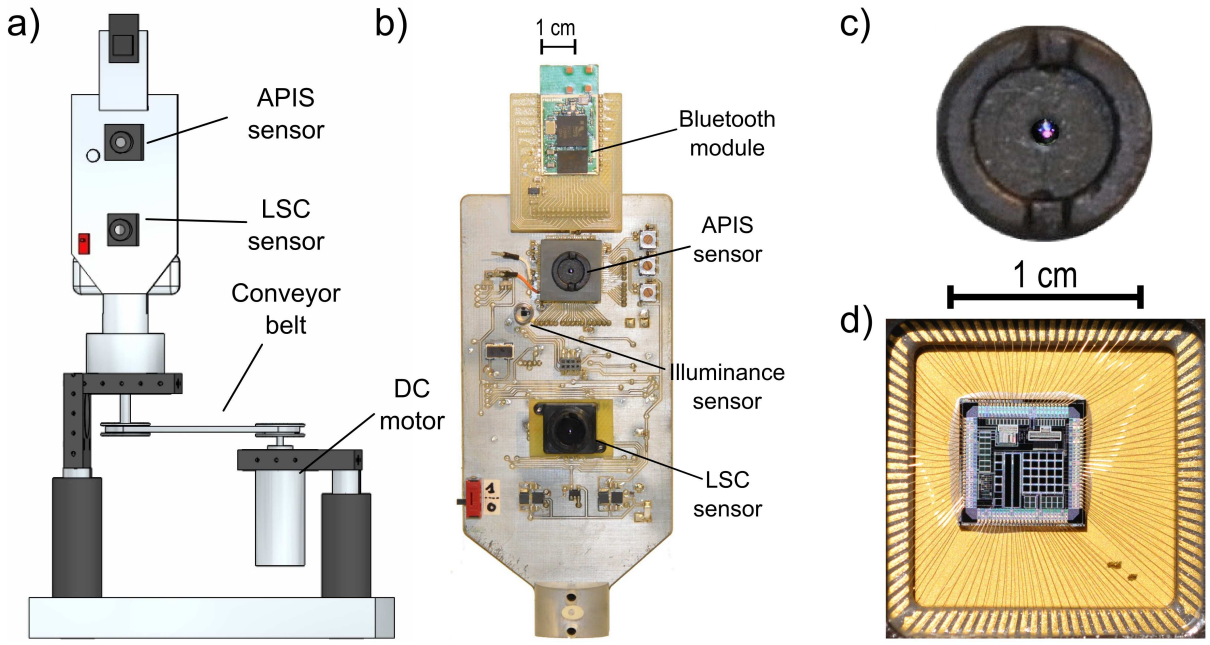

Figure 2: Test-board that includes both local motion sensors
a) Sketch of the full mechanical system. A mechanical rotational angular speed Ω was imposed on the board by means of a DC motor (2233012S from Minimotor) regulated via a proportional-integral controller.
b) Picture of the sensor board, which included the two custom-made visual motion sensors, an illuminance sensor based on a single elementary photodiode, and on the other side of the board (not visible here), a rate gyro (Analog Devices, ADIS 16100) measuring the reference mechanical angular speed (i.e., the rotational speed of the board) and a 16-bit microcontroller (dsPIC 33FJ128GP804) equipped with several 12-bit ADC (Analog to Digital Converter) inputs. The microcontroller processes the visual signals received by the two visual motion sensors at a sampling frequency of 2kHz. The measured visual motion ω_{meas} and the rotational speed Ω_{gyro} are recorded synchronously and sent to a computer via a Bluetooth module connected to a small battery (LiPo, 300mAh-3.3V). This wireless link leaves the sensor board free to rotate autonomously.
c) The visual motion sensors' miniature camera lens (Sparkfun SEN-00637, focal length 2mm, f-number 2.8) is defocused with respect to the focal plane to create a Gaussian angular sensitivity.
d) The APIS sensor along with the 5x5 photodiode array and an auto-adaptive circuit: only two pixels are connected to the dsPIC microcontroller.

features an integrated photodiode with a sensitive area of $250\mu m * 250\mu m$ connected to an adaptive, time-continuous, logarithmic circuit having a dynamic range of 100dB.

The front-end of the LSC-based local motion sensor was based on an off-the-shelf photodiode array (LSC is a component purchased from iC-Haus) consisting of 2 rows of 6 pixels. To make the sensor able to distinguish a larger number of contrasting patterns at low illuminance levels, we summed together the 2 pixels in the same column to improve the signal-to-noise ratio by increasing the sensitive area to $300\mu m * 1600\mu m$. These two "elongated photosensors" were combined with a classical fixed-gain photocurrent amplifier implemented using Surface Mount Device (SMD) components. The original local motion detector (Blanes, 1986; Franceschini et al., 2009; Ruffier et al., 2003) (also called "time of travel") consisted of an analog circuit producing an output signal that increased as the time lag Δt between its two inputs decreased. The output signal therefore increased with the angular speed ω. Like the fly's motion-detecting neurons from which it was originally inspired (Franceschini et al., 1989), our visual motion sensors can react to either dark-to-light (ON) or light-to-dark (OFF) contrasts. The bio-inspired signal processing method implemented in each of the two local motion sensors can be decomposed into 6 steps (Blanes, 1986; Franceschini et al., 2009; Ruffier et al., 2003) (see figure 1) as follows:

- Step 1: Spatial sampling and low-pass spatial filtering (which is achieved by defocusing the miniature camera lens to obtain a Gaussian angular sensitivity for each pixel),
- Step 2: Band-pass temporal filtering: high-pass temporal filtering to differentiate the visual signals and low-pass temporal filtering to reduce the noise such as the 100-Hz interference originating from artificial lighting (this step is partially analog in the case of the LSC-based visual motion sensor),
- Step 3: Taking the absolute value of the signals to detect both dark-to-light and light-to-dark contrast transitions,
- Step 4: Thresholding with fixed values regardless of the illuminance background,
- Step 5: Measuring the time Δt (time of travel) elapsing between the thresholded signals,
- Step 6: Computing the local angular speed by applying:

$$\omega_{meas} = \frac{\Delta\varphi}{\Delta t} \tag{1}$$

Each angular speed measured was then fed via a tiny Bluetooth module (F2M03GLA from Free2move company) into a computer for analysis.

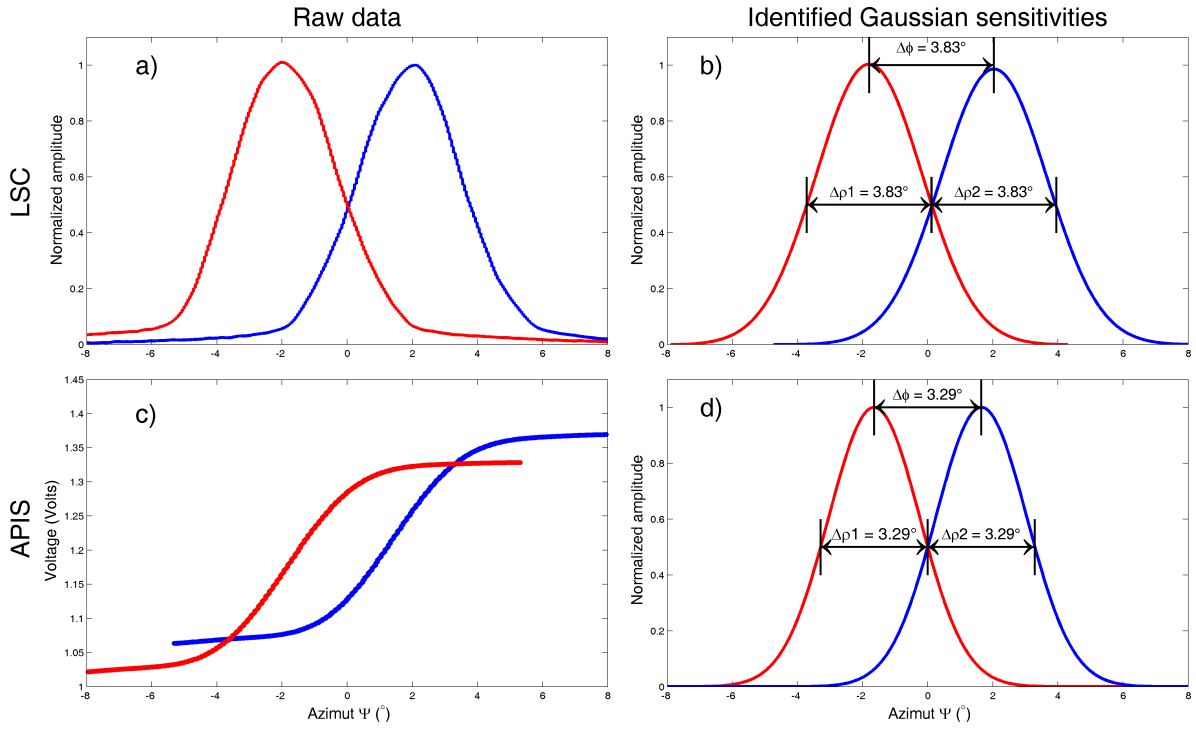

Figure 3: Gaussian angular sensitivities of the LSC and APIS photosensors
a) Outputs of the two linearly amplified photosensors in the LSC array during a slow rotation of the sensor placed 50cm in front of a fixed point light source.
b) Gaussian sensitivity of the two photodetectors approximated using *cftool* (Matlab). The defocusing was adjusted in order to obtain $\Delta\varphi = \Delta\rho$. As the correlation coefficient ($R^2_{LSC} > 0.994$) is very nearly equal to 1, this confirms that we can obtain Gaussian sensitivity by defocusing.
c) Outputs from the two photosensors used out of the 25 pixels on the APIS retina, when rotated horizontally in front of a vertical black-and-white contrasting edge.
d) Gaussian sensitivity of the APIS photoreceptors computed from the approximated error function, erf ($R^2_{APIS} > 0.999$).

This overall processing was carried out on a dsPIC 33FJ128GP804 microcontroller working at a sampling frequency of 2kHz in floating-point arithmetic. The simultaneous processing of the two sensors (APIS-based and LSC-based) including the serial readout interface occupies 10% of the program memory, 13% of the data memory of the microcontroller and accounts for 52% of the processing time available at a sampling frequency of 2kHz. The overall signal processing tasks do not require performing any time-consuming tasks such as division because a look-up table was used to transform the Δt into the visually perceived angular speed ω_{meas} (see equation 1). All embedded algorithms were developed on Matlab with a Simulink blockset for dsPIC called Embedded Target for dsPIC.

The angular sensitivity function of a single fly photoreceptor is a Gaussian distribution (Götz, 1964), which results from the spatial convolution of the photoreceptor's diameter with the point spread function of the facet lenslet (Franceschini & Kirschfeld, 1971; Stavenga, 2003). As shown in figure 3, a similar Gaussian sensitivity profile to that of the fly was obtained here by defocusing the lens of a miniature camera (by reducing the distance between the lens and the retina). In each local motion sensor, the full width at half-height of the Gaussian curve (which is called the acceptance angle) $\Delta\rho$ directly determines the cut-off frequency of the low-pass spatial filtering process (step1), whereas the inter-receptor angle $\Delta\varphi$ determines the angular speed (ω) measurement range. As occurs in some diurnal insects (Land, 1997), these angles were adjusted in this study to obtain the following optical property:

$$\Delta\varphi = \Delta\rho \tag{2}$$

It is worth noting that these two optic sensors were both constructed using the same optic assembly originating from a low-cost miniature camera lens (Sparkfun SEN-00637, focal length 2mm, f-number 2.8).

In the case of the LSC-based photoreceptors, the angular sensitivity function of the lens/photodiode assembly was assessed by slowly rotating the photoreceptors placed 50cm in front of a fixed point light source. The angular sensitivity measured fitted a Gaussian curve (cf. figure 3a and b) having the width at half-height $\Delta\rho_{LSC} = 3.8^{\circ}$, the inter-receptor angle $\Delta\varphi_{LSC} = 3.8^{\circ}$and the correlation coefficient $R^2_{LSC} > 0.994$. In the case of the APIS-based photoreceptors, the angular sensitivity function of the lens/photodiode assembly was assessed from the Gaussian error function (cf. figures 3c and 3d) obtained by quickly rotating in the horizontal plane the visual motion sensor placed 1 meter in front of a vertical contrasting edge (Kerhuel, 2009). The correlation coefficient between the raw data and the Gaussian error function (erf) was $R^2_{APIS} > 0.999$ in this case when $\Delta\rho_{APIS} = \Delta\varphi_{APIS} = 3.3^{\circ}$.

The main characteristics of the two sensors are summarized in the table 1. In previous local motion sensors (Pudas, Kruusing, Leppavuori, Boyron, Amic, Viollet & Franceschini, 2007; Ruffier et al., 2003), the temporal band-pass filter consisted of a 1^{st} order high-pass filter with a cut-off frequency of 20Hz and a 4^{th} order Butterworth low-pass filter with a cut-off frequency of 30Hz. To reduce the processing burden on the microcontroller, the order of the Butterworth filter of both sensors was reduced two-fold thanks to the on-chip pre-amplification unit, which reduced

Table 1: Specifications of the APIS-based and LSC-based visual motion sensors.

Local motion Sensor	APIS-based	LSC-based
Inter-receptor angle $\Delta\varphi(^\circ)$	3.3	3.8
Acceptance angle $\Delta\rho(^\circ)$	3.3	3.8
Photodiode size (μm)	250 x 250	300 x 1600
Pixel pitch (μm)	300	420
Focal length of the lens (mm)	2	
F_{number} of the lens (#)	2.8	
Angular velocity Range ($^\circ$/s)	[50, 350]	
Resolution ($^\circ$/s) [Min; Max]	[0.4; 18.32]	[0.33; 15.14]
Sensitivity ($^\circ$/s/LSB)	1.53 e-3	
Estimated mass with optics in a stand-alone version (g)	$<$ 2g	$<$ 1g

the noise. A 2^{nd} order digital low-pass filter was therefore implemented in the dsPIC microcontroller (cf. figure 1). In addition, as the on-chip auto-adaptive circuit already features an illuminance-dependent high-pass filter effect, the cut-off frequency of the high-pass filter in the present APIS-based visual motion sensor was reduced to 5Hz.

Figure 2b shows the two local motion sensors mounted on an identical printed-circuit board (PCB). An additional illuminance sensor (an OSRAM photodiode BPX65) was connected to an analog amplifier circuit operating in the photovoltaic mode in order to measure the effective illuminance of the scene scanned by the visual motion sensors. The photocurrent I_{ph} output of this illuminance sensor was determined as follows:

$$I_{ph} = (e^{V_{out}/0.125} - 1)I_{dark} \tag{3}$$

where the dark current I_{dark} is equal to $1nA$ and V_{out} is the amplifier's output voltage (Riggs, 1983). The sensor board was rotated by means of a DC motor (see figure 2a) controlled by a proportional-integral regulator.

3 Benchmarking of the visual motion sensors

The two visual motion sensors were tested both indoors and outdoors (see figures 4a and 4b) by comparing their output signals with the angular speed Ω_{gyro} measured on a rate gyro (Analog Devices, ADIS 16100), which can measure angular speeds in the 0 to $300^\circ/s$ range. For the outdoor measurements, the sensor board was placed on a table equipped with 4 rugged wheels.

As shown in figure 2a, the sensor board was connected to a DC motor via a belt, which made it possible to finely adjust the mechanical angular speed of the board, Ω ranging between $60^\circ/s$ and $300^\circ/s$. In both environments,

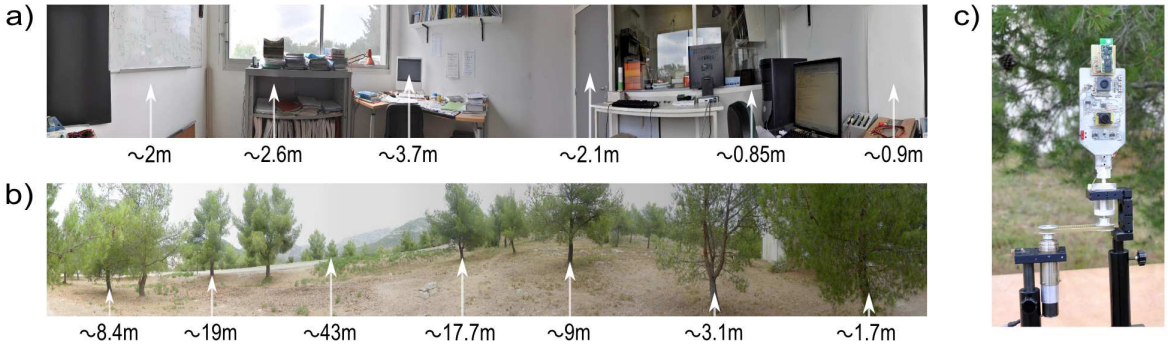

Figure 4: **a)** Picture of the indoor scene where the local motion sensors were tested.
b) Picture of the outdoor scene where the local motion sensors were tested. Distances to the surrounding objects (indicated by a white arrow) are given below each picture.
c) Picture of the sensor board and the mechanical system placed outdoors.

the static and dynamic responses of the visual motion sensors were measured with several background illuminance values:

- indoors: (i) 50lux, (ii) 2000-10000lux, corresponding to (i) a dim artificial light and (ii) a large amount of sunlight from the windows;
- outdoors: (i) 100lux, (ii) 10000lux, corresponding to (i) dusk and (ii) a sunny day.

The low illuminance values used indoors and outdoors were chosen to allow the LSC-based local motion sensor to detect contrasts and the high illuminance values were the maximum possible values obtained at this period of the year (April 2010) in Marseilles when a luxmeter was oriented at the same direction than the sensors. The background illuminance values were measured in lux by a digital lux-meter (Roline, RO-1332), which gives only an estimate of the overall environmental illuminance. The static responses of the sensors were assessed by applying a series of 30°/s fifteen-second steps at a rotational speed Ω ranging from $60°/s$ to $300°/s$. To test the dynamic characteristics of the sensors, a 50-second stimulus was applied, during which variably long periods of constantly increasing and decreasing velocity ranging between $60°/s$ and $300°/s$ were imposed.

4 Experimental results

4.1 Static angular speed characteristics

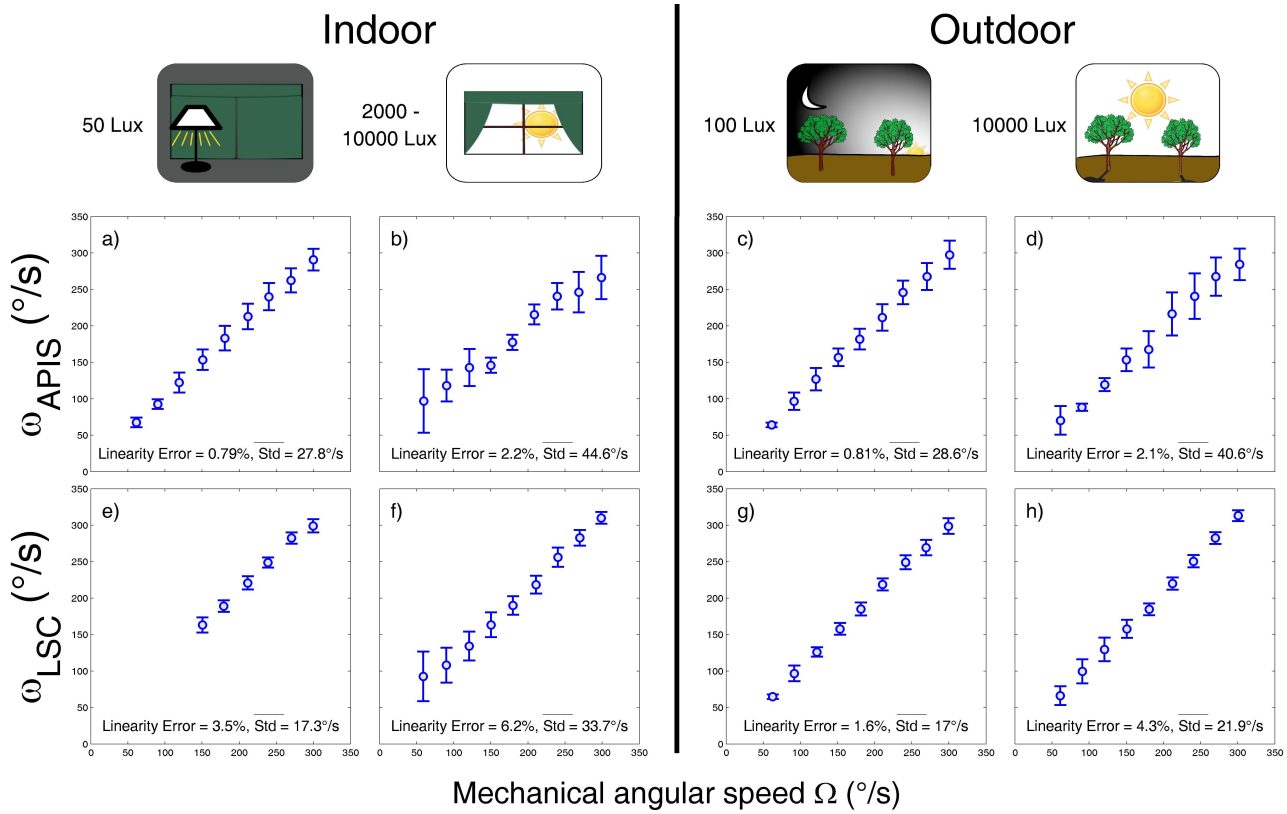

Figure 5: Static indoor and outdoor characteristics of the LSC- and APIS-based local motion sensors assessed by applying $30°/s$ steps (lasting 15 seconds) to the rotational speed from $60°/s$ to $300°/s$. The background illuminance ranged indoors between 50lux and 2000lux (apart from some peaks at 10000lux) and outdoors between 100lux and 10000lux. The mean visual motion recorded at each angular speed Ω is plotted in this figure with its standard deviation. The best linear approximation obtained in each experiment was computed and the departure from linearity is given as a percentage.

a-b-c-d) Static indoor and outdoor characteristics of the APIS-based local motion sensor.

e-f-g-h) Static indoor and outdoor characteristics of the LSC-based local motion sensor.

b-d) When the illuminance increased, the dispersion of the data recorded with the APIS-based visual motion sensor increased due to several matching errors occurring because of the adaptation process of the auto-adaptive circuit at work during the data capture.

e) At low angular speeds and low illuminance values, the LSC-based local motion sensor did not detect any contrasts during the 15-second steps.

f-g-h) The LSC-based local motion sensor responded as soon as the background illuminance values and the rotational speed were high enough. In addition, the LSC-based local motion sensor showed good linearity and little dispersion.

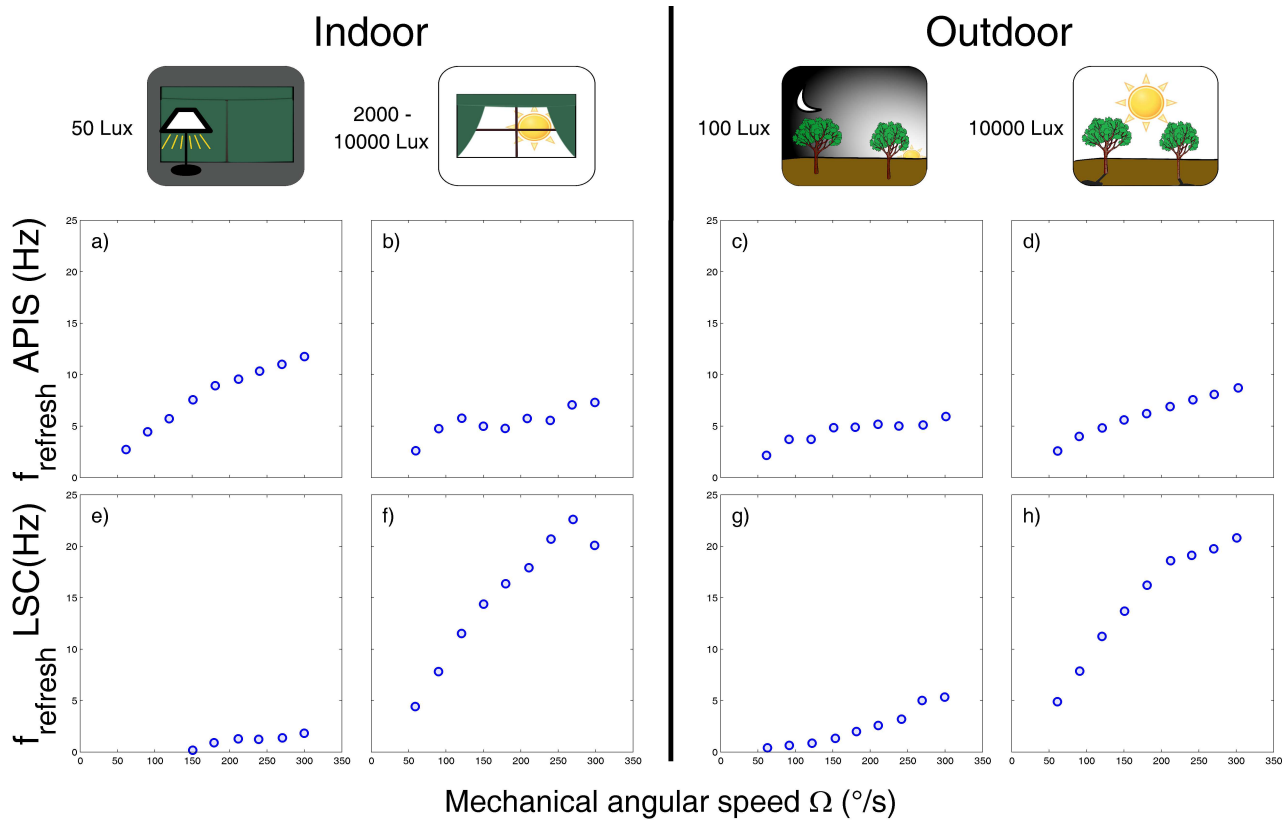

Figure 6: Refresh rates of the LSC- and APIS-based local motion sensors measured indoors and outdoors at a rotational speed ranging from $60°/s$ to $300°/s$ in $30°/s$ steps (lasting 15s).
a-b-c-d) Refresh rate of the APIS-based local motion sensor indoors and outdoors with an illuminance background varying from 50lux to 10000lux. The on-chip auto-adaptive circuit rendered the APIS-based local motion sensor invariant to the illuminance in terms of the refresh rate.
e-f-g-h) Refresh rate of the LSC-based local motion sensor indoors and outdoors with an illuminance background ranging from 50lux to 10000lux. The LSC-based local motion sensor showed the occurrence of considerable refresh rate variations at several illuminance levels. The LSC-based local motion sensor was found to have much higher refresh rates at high illuminance values than the APIS-based visual sensor.

Figure 5 gives the static characteristics of the two sensors indoors and outdoors, as assessed by applying $30°/s$ steps (lasting 15 seconds) to the rotational speed from $60°/s$ to $300°/s$. The background illuminance ranged indoors between 50lux and 2000lux (apart from some peaks at 10000lux) and outdoors between 100lux and 10000lux. With each visual motion sensor and at each illuminance level, the mean standard deviation of the data was computed as follows:

$$\overline{Std} = \overline{std(\omega_{meas})} \tag{4}$$

To estimate the accuracy of the sensor, the best linear approximation was calculated with each sensor and each illuminance background, based on the equation 5.

$$\omega_{meas} = a \times \Omega \tag{5}$$

The regression coefficient of this function was used to compute the linearity error according to the equation 6.

$$LinearityError(\%) = |(a-1)| \times 100 \tag{6}$$

As shown in figure 5, the LSC-based local motion sensor showed a high level of invariance to the illuminance, while the linearity of its static characteristics remained unchanged, provided the illuminance and the rotation speed were maintained at a relatively high level. Regardless of the illuminance, both sensors responded accurately, as shown by the small linearity error rate ($<$4.5% in most cases). As shown in figure 5e, the LSC-based local motion sensor remained silent at a 50-lux illuminance level and at rotational speeds below $150°/s$. The static characteristics of the APIS-based local motion sensor also showed good invariance to the lighting conditions, whereas the dispersion of the values increased slightly with the illuminance at the lowest and highest speeds tested (figures 5b and 5d).

The dispersion of the data obtained with the APIS-based local motion sensor was no doubt mainly attributable to the presence, at the pixel level, of an auto-adaptive circuit with no anti-aliasing filter. The digitization process may therefore have distorted the photodiode signals, thus causing visual motion measurement errors. The frequency response of the adaptive circuit showed a dramatic increase in the bandwidth with the illuminance, ranging from 700Hz at 1lux to 1MHz at 10^5lux.

4.2 Refresh rate analysis

The refresh rates of the two sensors measured indoors and outdoors are shown in Figure 6. The refresh rate was defined as the number of new motion measurements per second: a new measurement occurs when a contrast transition is detected by one pixel and then by the second pixel with a time lag Δt in our measurement range, corresponding to an angular speed in the [50°/s, 350°/s] range (see equation 1). A contrast was detected whenever

the two adjacent photodiode outputs exceeded the threshold values in the preferred direction. On the whole, the refresh rate of the LSC-based visual motion sensor was found to depend on the illuminance and to vary quasi-linearly with the rotational speed Ω_{gyro}.

Landolt and Mitros (Landolt & Mitros, 2001) have stated that an eye rotating at an angular speed ω converts spatial frequency into temporal frequency as given by the equation:

$$f_T = \omega \times f_S \tag{7}$$

(where f_T is the temporal frequency of the photoreceptor output signal, ω is the angular speed of the visual sensor with respect to the contrasting pattern, and f_S is the spatial frequency associated with the contrasting pattern).

According to the above equation 7 and assuming that the local motion sensor detected the same contrasts regardless of the angular speed, the number of new angular speed measurements per second could be expected to increase linearly with the rotational speed as the temporal frequency f_T increased. However, as shown by figures 6f and 6h, the refresh rate of the LSC-based visual motion sensor stopped increasing at high angular speeds. Spatial low-pass filtering (cf. figure 3) combined with a temporal second order low-pass filter (cf. figure 1) limited the range of the temporal frequency f_T of each photoreceptor output signal to a frequency of 30Hz and therefore limited the refresh rate of the LSC-based motion sensor to below 30Hz at high angular speeds.

Contrary to the refresh rates of the LSC-based motion sensor, which showed considerable variations (between 5Hz and 23Hz at 300°/s, see figures 6e, 6f, 6g and 6h), those of the APIS-based visual sensor were found to be independent of the illuminance and to increase slightly with the angular speed (see figures 6a, 6b, 6c and 6d). In each environmental condition, the illuminance background dispersion was computed from the illuminance sensor data recorded at each angular speed during the static experiments (figure 5 and 6). Based on the mean values obtained in each experiment, the dispersion was found to be quite low at low illuminance levels (58nA at 50lux and 1.3μA at 100lux) and greater at high illuminance levels (8.4mA at 2000-10000lux indoors and 1.1mA at 10000lux outdoors). Because of these marked variations in the background illuminance, the Delbrück's pixels in the APIS chip were constantly adapting to a new background illuminance with a relatively slow time constant varying with the illuminance (from $\sim 10\mu$s at 100lux to $\sim$ 1ms at 10000lux). Therefore, during the tests, the photoreceptor output signals frequently exceeded the switch-on point of the hysteresis function (step 4 in figure 1) without dropping fast enough below the switch-off point before the next contrast was encountered. A linear increase in the angular speed therefore did not lead to a linear increase in the APIS-based motion sensor's refresh rate. The switch-on and switch-off points of the hysteresis threshold function in the APIS-based motion sensor were selected because they gave the best trade-off between its refresh rate and the angular speed measurement accuracy.

4.3 Dynamic visual motion characteristics

The dynamic indoor and outdoor responses of the two visual motion sensors are shown in figure 7, where the angular speed ω_{LSC}, ω_{APIS} measured (blue dots) is superimposed on the reference angular speed Ω_{gyro} (red). In the dynamic experiments, the data dispersion was taken to be the standard deviation of the difference between the angular speeds measured by the rate gyro and the local motion sensor output signal, according to the following equation 8:

$$Std_{error} = std(\Omega_{gyro} - \omega_{meas}) \tag{8}$$

Despite the great difference in the illuminance, which ranged between 50lux and 10000lux (figures 7i, 7j, 7k and 7l), the responses of both the APIS and LSC-based visual motion sensors faithfully obeyed the triangular law imposed on the rotational speed of the board. During the indoor experiment at 2000lux, as the light coming mainly from a single window was non-uniformly distributed, strong variations in the illuminance (between 2000 and 10000lux) were observed during a 360° rotation, as shown in figure 7j.

As shown in figures 7b and 7d, the error and the standard deviation of the APIS-based local motion sensor increased slightly with the illuminance.

At low illuminance levels, the average refresh rate of the LSC-based motion sensor was below 3Hz (7e and 7g). As the illuminance increased, the average refresh rate $\overline{f_{refresh}}$ of the LSC-based local motion sensor increased without strongly increasing the corresponding standard deviation (figures 7f and 7h). As mentioned above in connection with the static measurements, the APIS-based motion sensor's refresh rate increased slightly with the illuminance, whereas the refresh rate of the LSC-based motion sensor increased from 1.26Hz to 15.3Hz between 100lux and 10000lux.

Local motion sensors with average refresh rates greater than 6Hz and standard deviations below 50°/s can be said to constitute remarkable tools for performing robotic tasks such as obstacle avoidance or terrain following. It can therefore be seen from figures 5-6-7 that the LSC- and APIS-based local motion sensors are both highly suitable for performing tasks of this kind even outdoors at illuminance levels ranging between 300-10000lux (1.5 decades) and 10-10000lux (3 decades), respectively.

5 Conclusion

Two 1-D visual motion sensors were tested and characterized here in field experiments under various lighting conditions. The benchmark test presented above can be used to fully characterize various visual motion sensors

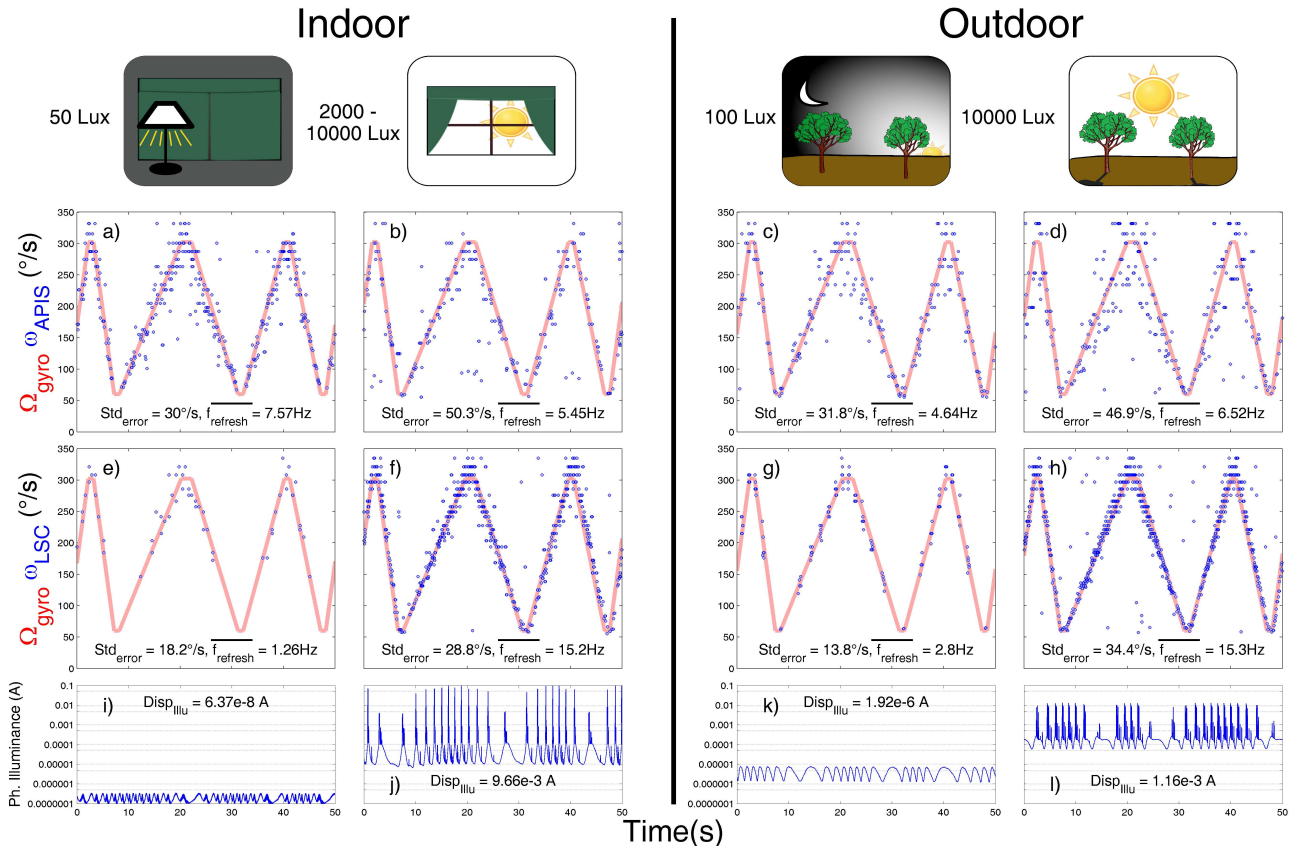

Figure 7: Dynamic indoor and outdoor responses of the two visual motion sensors (blue dots, figure 4a and 4b). The visual motion sensors mechanically rotated, giving a triangular pattern of angular speed variation (red) involving a series of velocity ramps ranging between 60°/s and 300°/s with different slopes under four different lighting conditions. Despite the strong illuminance variations, both visual motion sensors followed the rotational angular speed quite faithfully. With both sensors, the error between the measured local motion ω_{meas} and the angular velocity measured by the rate gyro Ω_{gyro} was used to compute the standard deviation of the error. The average refresh rate of the sensor was defined here as the number of new measurements occurring during the whole experiment divided by the duration of the experiment.

a-b-c-d) Dynamic indoor and outdoor responses of the APIS-based local motion sensor. Despite the considerable variations in the illuminance, the average refresh rate of the APIS-based sensor was always of a similar order of magnitude thanks to the auto-adaptive circuit. As shown in (b) and (d), the standard deviation of the error increased with the illuminance.

e-f-g-h) Dynamic indoor and outdoor responses of the LSC-based local motion sensor. As was to be expected from the static characteristics, the average refresh rate of the LSC-based sensor can be seen in these figures to have increased with the illuminance.

i-j-k-l) Dynamic response of the illuminance sensor and dispersion of the photodiode's output current. The large variations in the values detected by the illuminance sensor shown in (j) and (l) increased the dispersion of the APIS-based local motion sensor's response as shown in (b) and (d).

indoors and outdoors under several decades of illuminance. The performances of the visual motion sensors tested with this method can be said to correspond fairly well to those which could be obtained with a flying robot because the sensors were tested here in field experiments under various lighting conditions.

As expected in view of its auto-adaptive pixels, the APIS-based local motion sensor based on a custom-made VLSI retina equipped with adaptive pixels gave the best performances in terms of its invariance to the illuminance. Although the LSC-based local motion sensor equipped with linearly amplified photosensors failed to respond to contrasts encountered at low angular speeds ($<150°/s$) under low illuminance conditions (<300lux), all its measurements were highly accurate. Thanks to the auto-adaptive circuit designed to detect visual motion in several decades of illuminance, the characteristics of the APIS-based motion sensor are fairly consistent in this range, although some improvements could be made in terms of the average refresh rate and the accuracy. In the new APIS chip, it is proposed to integrate in the future an additional first order low-pass filter at the pixel level to decrease the dispersion of the APIS-based motion sensor.

The average refresh rate of the visual motion sensors, which is a key parameter in visual control systems based on motion sensors, was studied in particular here. It was established that the LSC-based motion sensor gives higher refresh rates at high angular speeds and strong illuminance levels than the APIS-based motion sensor. However, the average refresh rate of the latter sensor endowed with auto-adaptative pixels is suitably high even at low illuminance levels.

The LSC-based motion sensor gave the best results in terms of the accuracy and the average refresh rate in a narrow illuminance range (1.5 decades), whereas the APIS-based motion sensor turned out to be capable of measuring the angular speed in a 3-decade range of illuminance values.

To summarize, it was established here that these miniature visual motion sensors consisting of low cost optics and classical electronic components combined with appropriate visual signal processing methods give accurate and reliable results under natural conditions even in an outdoor environment. Besides, the "time of travel" scheme along with fixed thresholds and settings proved to be efficient in an illuminance range of several decades. In this study, we focused consistently on the same parameters in order to be able to make valid comparisons, but the performances of the sensors could be improved by dynamically adjusting the thresholds, (see figure 1, step 4) depending on the illuminance.

A stand-alone version of these sensors will predictably weigh less than 2g in the case of LSC-based and APIS-based local motion sensors.

These sensors could be used in natural environments on aerial or terrestrial robots for obstacle avoidance, take-off and landing, speed control purposes. Depending on what type of robotic behaviour is required, the Gaussian angular

sensitivity has to be adjusted to fit a specific altitude and speed range. The inter-receptor and acceptance angles determine the most suitable distance at which objects should be detected, and thus the angular speed range that can be measured on the basis of the motion sensor's range. In our case, a similar visual motion sensor ($\Delta\varphi = \Delta\rho = 4^\circ$) to those tested here has been successfully used on the aerial robot OCTAVE (Ruffier & Franceschini, 2005), which was able to fly at altitudes of up to 1.5m and speeds of up to 3m/s.

Depending on the field of application for which visual motion sensors are intended, great care has to be taken in choosing appropriate electronic circuits at the pixel level. It was established in this study that auto-adaptive pixels do not always yield the most accurate measurements in terms of the angular speed. In conclusion, this study brings us one step further towards implementing tiny, light, robust visual motion sensors that could be applied in many fields such as automotive, robotic and avionic design, planetary landers and free-flying micro-aerial vehicles weighing less than 10 grams.

Acknowledgements

We are most grateful to M. Boyron for the electronic design, Y. Luparini and J. Diperi for the mechanical design, F. Roubieu for the panoramic views of the indoor and outdoor environments, M. Menouni, F. Aubepart, G. Portelli and N. Franceschini for their fruitful comments and suggestions during this study and Dr. Jessica Blanc for correcting the English manuscript. We are grateful to the three anonymous referees for their relevant suggestions, which have greatly improved the manuscript. This research was supported partly by CNRS (Life Science; Information and Engineering Science and Technology), Aix-Marseille University II, the French National Research Agency -ANR- (EVA project under ANR-ContInt grant number ANR-08-CORD-007-04) and the European Commission via the CURVACE project. The project CURVACE acknowledges the financial support of the Future and Emerging Technologies (FET) programme, within the Seventh Framework Programme for Research of the European Commission, under FET-Open grant number: 237940.

References

Aubépart, F., Ménouni, M., Loubignac, T., Dinkelspieler, B., & Franceschini, N. (2007). Capteur de flux optique basé sur une rétine intégrée et un FPGA. In *Colloque Interdisciplinaire en Instrumentation*, (pp. 508–520). Hermes.

Barron, J., Fleet, D., & Beauchemin, S. (1994). Performance of optical flow techniques. *International Journal of Computer Vision*, *12*, 43–77.

Barrows, G. & Neely, C. (2000). Mixed-mode VLSI optic flow sensors for in-flight control of a Micro Air Vehicle. *in SPIE : Critical technologies for the future of computing, San Diego, CA, USA*, *4109*, 52–63.

Benson, R. & Delbrück, T. (1992). *Advances in Neurul Information Processing Systems*, chapter Direction selective silicon retina that uses null inhibition, (pp. 756–763). D. S. Touretzky, Ed. San Mateo, CA: Morgan Kaufman,.

Beyeler, A., Zufferey, J.-C., & Floreano, D. (2009). Vision-based control of near-obstacle flight. *Autonomous robots*, *27*(3), 201–219.

Blanes, C. (1986). Appareil visuel elementaire pour la navigation à vue d'un robot mobile autonome. Master's thesis, in Neuroscience, Univ. of Marseille, France.

Blanes, C. (1991). *Guidage visuel d'un robot mobile autonome d'inspiration biologique 2nde Partie*. PhD thesis, Institut National Polytechnique de Grenoble (INP Grenoble).

Brinkworth, R., Shoemaker, P., & O'Caroll, D. (2009). Characterization of a neuromorphic motion detection chip based on insect visual system. *in 5th International Conference on Intelligent Sensors, Sensor Networks and Information Processing (ISSNIP), Melbourne, VIC, Australia*, 289–294.

Chan, R., Mulla, A., & Stol, K. (2010). Characterisation of low-cost optical flow sensors. *in Proceeding of the Australasian Conference on Robotics and Automation, Brisbane, Australia*, 1–8.

Dahmen, H., Millers, A., & Mallot, H. A. (2009). *Flying insects and robots*, chapter 9 : Insect inspired odometry by optic flow recorded with optical mouse chips, (pp. 115–126). Springer, Berlin, Eds : Floreano, D. and Zufferey,J. C. and Srinivasan, M. V. and Ellington, C.

Delbrück, T. & Mead, C. A. (1994). Adaptive photoreceptor with wide dynamic range. *in IEEE International Symposium on Circuits and Systems (ISCAS), London, UK*, *4*, 339–342.

Díaz, J., Ros, E., Agis, R., & Bernier, J. (2008). Superpipelined high-performance optical-flow computation architecture. *Computer Vision and Image Understanding*, *112*, 262–273.

Etienne-Cummings, R. (1999). Intelligent robot vision sensors in VLSI. *Autonomous Robots*, *7*, 225–237.

Franceschini, N. & Kirschfeld, K. (1971). In vivo optical study of photoreceptor elements in the compound eye of drosophila. *Biological Cybernetics*, *8*, 1–13.

Franceschini, N., Pichon, J. M., & Blanes, C. (1992). From insect vision to robot vision. *Philosophical Transactions of the Royal Society B: Biological Sciences*, *337*, 283–294.

Franceschini, N., Riehle, A., & Nestour, A. L. (1989). *Facets of Vision*, chapter 17 : Directionally Selective Motion Detection by Insect Neurons, (pp. 360–390). Springer, Berlin, Eds : D.G. Stavenga, R.C. Hardie.

Franceschini, N., Ruffier, F., & Serres, J. (2007). A bio-inspired flying robot sheds light on insect piloting abilities. *Current Biology*, *17*, 329 – 335.

Franceschini, N., Ruffier, F., Serres, J., & Viollet, S. (2009). *Aerial vehicles*, chapter 35 : Optic flow based visual guidance: from flying insects to miniature aerial vehicles, (pp. 747–770). Vienna : In-Tech, Eds : T. M. Lam.

Garratt, M. & Chahl, J. (2008). Vision-based terrain following for an unmanned rotorcraft. *Journal of Field Robotics*, *25*, 284–301.

Götz, K. (1964). Optomotorische Untersuchung des visuellen systems einiger Augenmutanten der Fruchtfliege Drosophila. *Biological Cybernetics*, *2*, 77–92.

Green, W., Oh, P., & Barrows, G. (2004). Flying insect inspired vision for autonomous aerial robot maneuvers in near-earth environments. *in IEEE International Conference on Robotics & Automation (ICRA), New Orleans, LA, USA*, *3*, 2347 – 2352.

Griffiths, S., Saunders, J., Curtis, A., Barber, B., McLain, T., & Beard, R. (2006). Maximizing miniature aerial vehicles. *IEEE Robotics and Automation Magazine*, *13*(3), 34–43.

Harrison, R. R. & Koch, C. (1999). A robust analog VLSI motion sensor based on the visual system of the fly. *Autonomous robots*, *7*(3), 211–224.

Hassenstein, B. & Reichardt, W. (1956). Systemtheoretische Analyse der Zeit-, Reihenfolgen-, und Vorzeichenauswertung bei der Bewegungsperzeption des Rüsselkafers. *Chlorophanus. Zeitschrift für Naturforschung*, *11*, 513–524.

Herisse, B., Russotto, F., Hamel, T., & Mahony, R. (2008). Hovering flight and vertical landing control of a VTOL unmanned aerial vehicle using optical flow. *in Proceedings of IEEE/RSJ International Conference on Intelligent Robots and Systems (IROS), Nice, France*, 1404–1409.

Higgins, C. & Shams, S. (2002). A biologically inspired modular VLSI system for visual measurement of self-motion. *IEEE Sensors*, *2*, 508–528.

Humbert, S. & Hyslop, A. (2010). Bioinspired visuomotor convergence. *IEEE Transactions on Robotics*, *26*, 121–130.

Iida, F. (2001). Goal-directed navigation of an autonomous flying robot using biologically inspired cheap vision. *in Proceedings of the 32nd International Symposium on Robotics (ISR), Seoul, SK*, 1404–1409.

Jackson, J. D., Callahan, D. W., & Marstrander, J. (2007). A rationale for the use of optical mice chips for economic and accurate vehicle tracking. *Proc. IEEE International Conference on Automation Science and Engineering CASE 2007, Scottsdale, AZ, USA*, 939–944.

Kendoul, F., Nonami, K., Fantoni, I., & Lozano, R. (2009). An adaptive vision-based autopilot for mini flying machines guidance, navigation and control. *Autonomous robots*, *27*, 165–188.

Kendoul, F., Yu, Z., & Nonami, K. (2010). Guidance and nonlinear control system for autonomous flight of minirotorcraft unmanned aerial vehicles. *Journal of Field Robotics*, *27*, 311–334.

Kerhuel, L. (2009). *Capteurs optiques minimalistes et réflexes oculomoteurs biomimétiques. Applications à la robotique aérienne*. PhD thesis, University of Montpellier, France.

Kerhuel, L., Viollet, S., & Franceschini, N. (2010). Steering by gazing: An efficient biomimetic control strategy for visually guided micro aerial vehicles. *IEEE Transactions on Robotics*, *26*, 307–319.

Koenderink, J. & van Doorn, A. (1987). Facts on optic flow. *Biological Cybernetics*, *56*, 247–254.

Kramer, J., Sarpeshkar, R., & Koch, C. (1995). An analog VLSI velocity sensor. *in Proceedings of the* IEEE *International Symposium on Circuit and Systems (ISCAS), Seattle, WA, USA*, 413–416.

Land, M. F. (1997). Visual acuity in insects. *Annual Review of Entomology*, *42*, 147–177.

Landolt, A. & Mitros, A. (2001). Visual sensor with resolution enhancement by mechanical vibrations. *Autonomous Robots, 11 (3)*, 233–239.

Laviana, R., Carranza, L., Vargas, S., Linan, G., & Roca, E. (2005). A bioinspired vision chip architecture for collision detection in automotive applications. *in Proceedings of SPIE : Bioengineered and bioinspired systems II,Sevilla, Espana*, *5839*, 13–24.

Liu, S. & Usseglio-Viretta, A. (2001). Fly-like visuomotor responses of a robot using aVLSI motion-sensitive chips. *Biological Cybernetics*, *85*, 449–457.

Mead, C. (1989). *Analog* VLSI *and Neural Systems*. Addison-Wesley.

Moeckel, R. & Liu, S. (2007). Motion detection circuits for a time-to-travel algorithm. *IEEE International Symposium on Circuits and Systems. (ISCAS), New orleans, LA, USA*, 3079–3082.

Moini, A. (1999). *Vision Chips*. Kluwer academic, Norwell, MA.

Netter, T. & Franceschini, N. (2002). A robotic aircraft that follows terrain using a neuromorphic eye. *in Proceedings of IEEE Conference on Intelligent Robots and Systems (IROS), Lausanne, Switzerland*, 129–134.

Okuno, H. & Yagi, T. (2009). A mixed analog-digital vision sensor for detecting objects approaching on a collision course. *Robotics and Autonomous Systems*, *57*, 508–516.

Orchard, G., Bartolozzi, C., & Indiveri, G. (2009). Applying neuromorphic vision sensors to planetary landing tasks. *in Biomedical Circuits and Systems Conference (BioCAS), Beijing, China*, 201–204.

Pudas, M., Kruusing, A., Leppavuori, S., Boyron, M., Amic, S., Viollet, S., & Franceschini, N. (2007). A miniature bio-inspired optic flow sensor based on low temperature co-fired ceramics (LTCC) technology. *Sensors and Actuator A: Physical*, *133*, 88–95.

Riggs, J. (1983). Notes on silicon photodiode detectors. *International Amateur-Professional Photoelectric Photometry Communications*, *14*, 30–44.

Ruffier, F. & Franceschini, N. (2005). Optic flow regulation: the key to aircraft automatic guidance. *Robotics and Autonomous Systems, 50(4)*, 177–194.

Ruffier, F. & Franceschini, N. (2008). Aerial robot piloted in steep relief by optic flow sensors. *in International Conference on Intelligent Robots and Systems (IROS), Nice, France*, 1266 – 1273.

Ruffier, F., Viollet, S., Amic, S., & Franceschini, N. (2003). Bio-inspired optical flow circuits for the visual guidance of micro-air vehicles. *Proceeding of IEEE International Symposium on Circuits and Systems (ISCAS), Bangkok, Thailand*, *3*, 846–849.

Santos-Victor, J., Sandini, G., Curotto, F., & Garibaldi, S. (1995). Divergent stereo in autonomous navigation: From bees to robots. *International Journal of Computer Vision*, *14*, 159–177.

Sarpeshkar, R., Bair, W., & Koch, C. (1993). Visual motion computation in analog VLSI using pulses. *Advances in Neural Information Processing Systems 5 (NIPS), Denver, CO, USA*, 781–788.

Sarpeshkar, R., Kramer, J., Indiveri, G., & Koch, C. (1996). Analog vlsi architectures for motion processing: From fundamental limits to system applications. *Proceedings of the IEEE*, *84 (7)*, 969–987.

Srinivasan, M. (1994). An image-interpolation technique for the computation of optic flow and egomotion. *Biological Cybernetics*, *71*, 401–415.

Stavenga, D. G. (2003). Angular and spectral sensitivity of fly photoreceptors. I. integrated facet lens and rhabdomere optics. *Journal of Comparative Physiology A*, *189*(1), 1–17.

Stocker, A. (2006). Analog integrated 2-D optical flow sensor. *Analog Integrated Circuits and Signal Processing*, *46*, 121–138.

Ullman, S. (1981). Analysis of visual motion by biological and computer systems. *Computer*, *14*, 57–69.

Viollet, S. & Franceschini, N. (1999). Biologically-inspired visual scanning sensor for stabilization and tracking. *in Proceeding IEEE/RSJ International Conference on Intelligent Robots and System (IROS), Kyongju, Korea*, 204–209.

Viollet, S. & Franceschini, N. (2001). Super-accurate visual control of an aerial minirobot. *in Autonomous Minirobots for Research and Edutainment (AMIRE), Paderborne, Germany*, 215–224.

Viollet, S., Ruffier, F., Ray, T., Menouni, M., Aubépart, F., Kerhuel, L., & Franceschini, N. (2010). Characteristics of three miniature bio-inspired optic flow sensors in natural environments. *in IEEE International Conference on Sensor Technologies and Applications (SENSORCOMM), Venice, Italy*, 51–55.

Xu, P., Humbert, J., & Abshire, P. (2011). Analog vlsi implementation of wide-field integration method. *Journal of Intelligent & Robotic Systems, Online*, 1–23.

Zufferey, J.-C. & Floreano, D. (2006). Fly-inspired visual steering of ultralight indoor aircraft. *IEEE Transactions on Robotics*, *22(1)*, 137–146.

Zwaan, S. & Santos-Victor, J. (1999). An insect inspired visual sensor for the autonomous navigation of a mobile robot. *in Proceeding of International Symposium on Intelligent Robotic Systems (SIRS), Coimbra, Portugal*, *1*, 1–10.